Supplemental Information

Improving the Long-term Stability of PBDTTPD Polymer Solar Cells Through Material Purification Aimed at Removing Organic Impurities

William R. Mateker,[a] Jessica D. Douglas,[b] Clément Cabanetos,[c] I.T. Sachs-Quintana,[a] Jonathan A. Bartelt,[a] Eric T. Hoke,[d] Abdulrahman El Labban,[c] Pierre M. Beaujuge,[c] Jean M.J. Fréchet[b,c] and Michael D. McGehee*[a]

[a]*Department of Materials Science and Engineering, Stanford University Stanford, CA 94305 USA.*
Email: mmcgehee@stanford.edu
[b]*Department of Chemistry, University of California Berkeley, CA 94720 USA.*
[c]*King Abdullah University of Science and Technology (KAUST) Thuwal, 23955-6900, Saudi Arabia.*
[d]*Department of Applied Physics, Stanford University Stanford, CA 94305 USA*

Section 1: Degradation in High M_n PBDTTPD Solar Cells

Table TS1: High M_n (Batch #H2) PBDTTPD Solar Cell Degradation

Device Parameter	Average Relative Values			
	Day 7	Day 14	Day 21	Day 28
J_{SC}	0.83	0.77	0.71	0.61
V_{OC}	0.99	0.99	0.99	0.97
Fill Factor	0.92	0.91	0.89	0.89
PCE	0.76	0.69	0.63	0.53

A large range in the relative J_{SC} loss was observed in high M_n PBDTTPD solar cells (Fig 3b). One source of the wide range of degradation could be a range of degradation among solar cells on one single substrate (Fig S1). To quantify the difference in degradation among devices on the same substrate, the relative degradation in J_{SC} was normalized to each substrate.

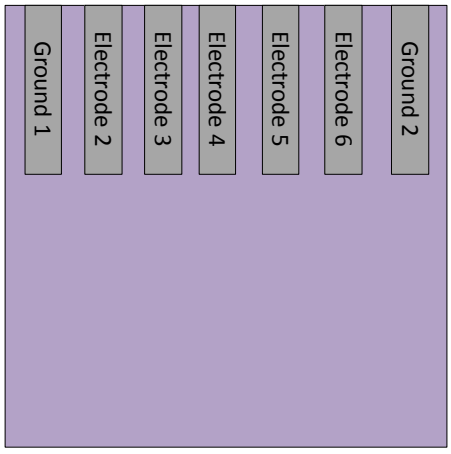

Figure S1: A schematic of a single substrate, which has 5 working solar cells. The electrodes on either end serve as grounds between the cathode and the ITO anode.

Sample values can be used as an illustrative example. After 28 days, the relative J_{SC} ($J_{SC,Aged}/J_{SC,\ Fresh}$) for devices 2-6 on one substrate were 0.80, 0.94, 0.75, 0.57, and 0.58. Dividing the relative J_{SC} loss for each device by the relative J_{SC} loss of device 3 gives the relative values of J_{SC} loss normalized for the substrate, which are 0.86, 1.0, 0.80, 0.61, and 0.63. Performing this analysis over all substrates reveals that, on average, electrode 4 degrades the least while electrodes 2 and 6 degrade the most (Fig. S2).

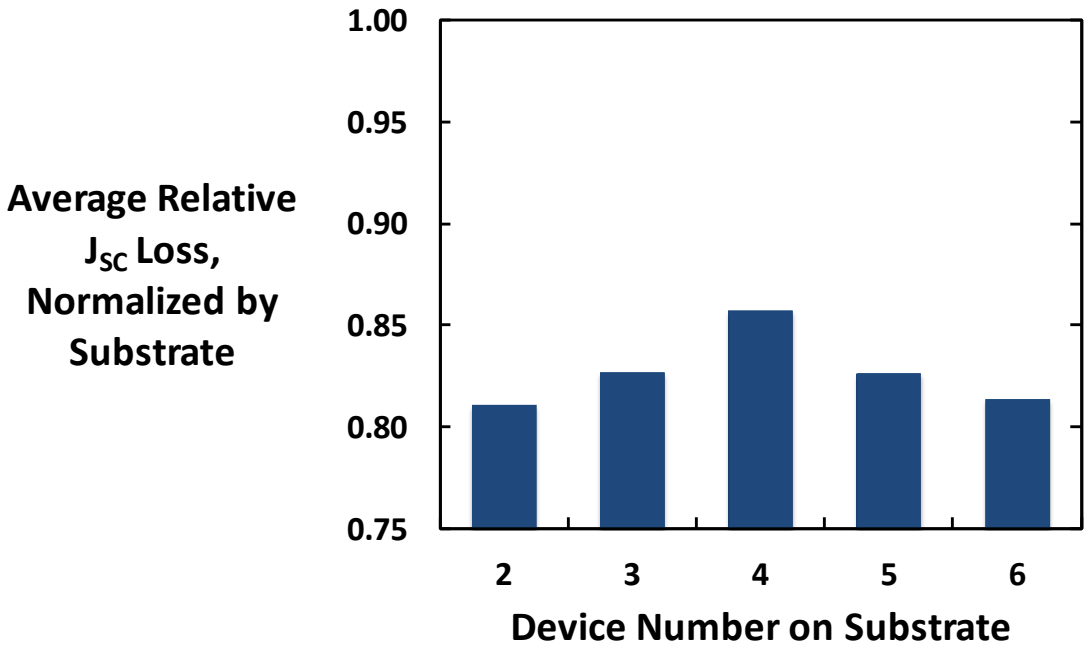

Figure S2: The relative J_{SC} loss, normalized for each substrate, was averaged over all substrates. On any given substrate, on average the middle electrode (4) degraded the least. The outer electrodes (2 and 6), on average, degraded the most.

Section 2: Degradation in Low M_n PBDTTPD Solar Cells

BHJ solar cells were fabricated from two separate batches of low M_n PBDTTPD. As discussed in the manuscript, their degradation under glovebox storage conditions differed from solar cells fabricated from high M_n PBDTTPD. Solar cells fabricated from low M_n PBDTTPD show less average PCE degradation than solar cells fabricated from high M_n PBDTTPD (10% in 7 days vs. 25%) (Fig. S3 and S4). They also show a smaller spread in J_{SC} degradation. Most notably, low M_n devices do not develop S-shapes in the reverse bias region of their J-V curves (Fig. S5).

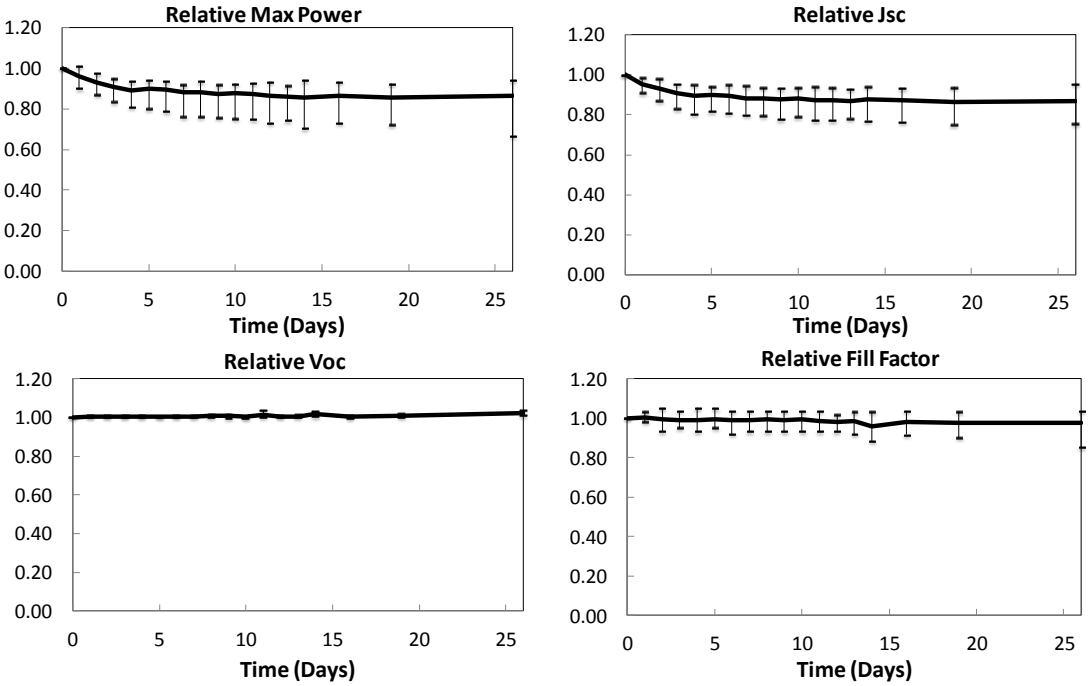

Figure S3: Degradation curves for low M_n (Batch #L1) PBDTTPD:$PC_{61}BM$ solar cells. The V_{OC} and fill factors of the devices are stable over the 26 days of daily testing, while the J_{SC} of the devices decrease under glovebox storage. The devices are more stable relative to their high M_n counterparts, and no devices formed the characteristic S-shape degradation feature.

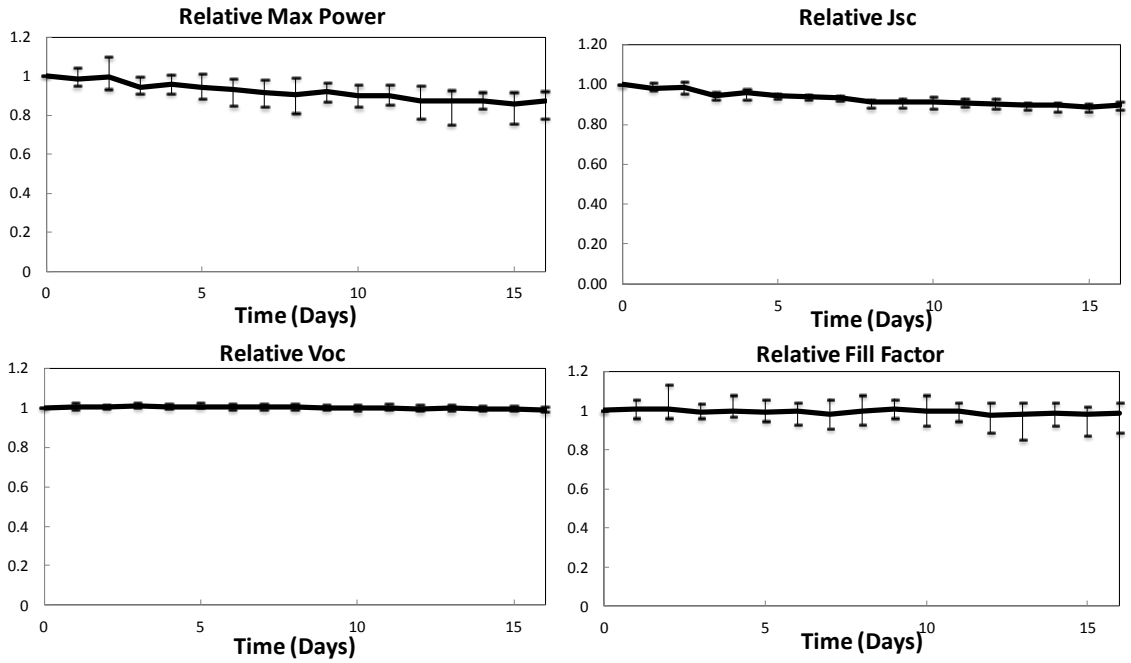

Figure S4: Degradation curves of BHJ solar cells fabricated from a second low M_n PBDTTPD polymer batch (Batch #L2). Device V_{OC} is stable, and the fill factor of a few devices even improves. The J_{SC} degrades by about 15% in 16 days. Despite this degradation in J_{SC}, S-shapes do not appear in any J-V curves of these low M_n PBDTTPD devices.

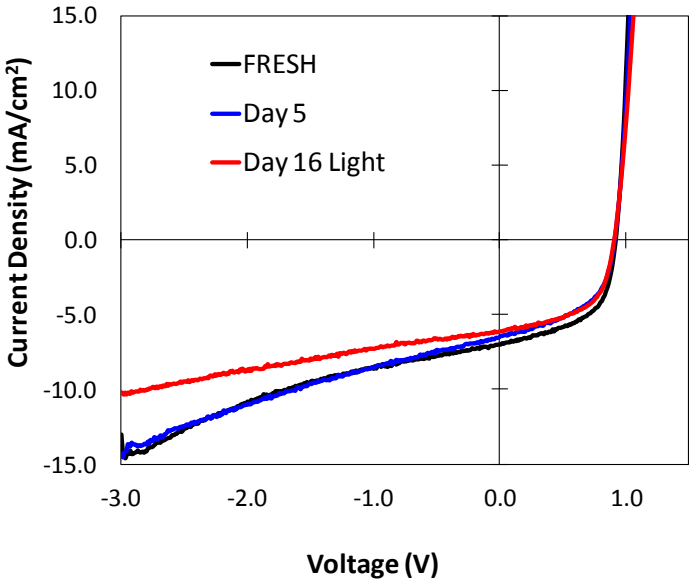

Figure S5: J-V curves of the most degraded BHJ solar cell fabricated from Batch #L2 of low M_n PBDTTPD after 16 days. There is no development of S-shapes in the reverse bias region.

Section 3: Switching the Cathode Material

We propose that an extraction barrier at the cathode causes the S-shape degradation symptom observed in illuminated J-V curves of high M_n PBDTTPD solar cells. All solar cells reported in this paper are in the standard architecture. The J-V curves of both the high and low M_n PBDTTPD presented in the text use ITO/PEDOT:PSS as the anode and Ca/Al as the cathode (Fig. S6).

Figure S6: A schematic for the device architecture of all solar cells presented in the manuscript.

In an attempt to prevent S-shape J-V curves from developing in high M_n PBDTTPD:$PC_{61}BM$ solar cells, we fabricated solar cells with a variety of different cathodes.

We fabricated solar cells without calcium, as calcium is highly reactive. First we fabricated solar cells with aluminum only cathodes. These unoptimized devices had slightly lower initial efficiencies, and suffered from poor stability (Fig. S7).

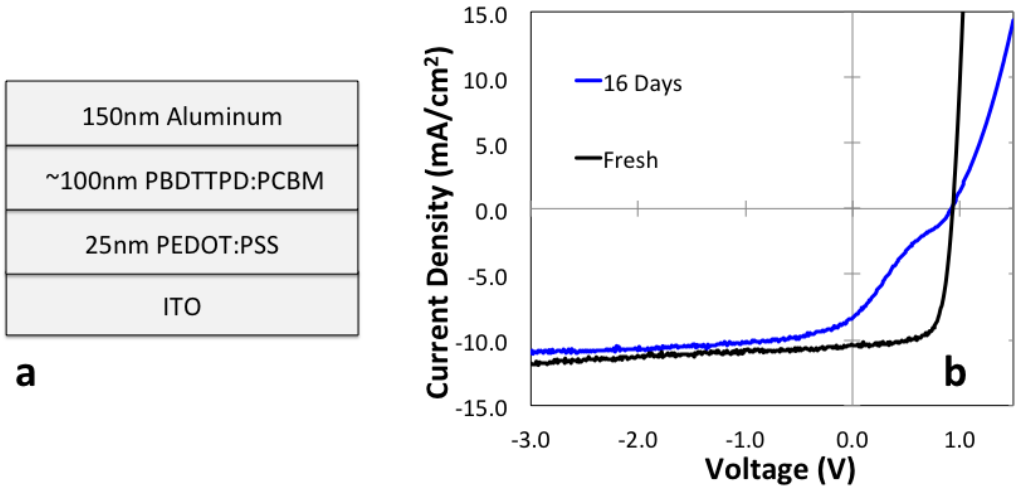

Figure S7: a) A schematic of a device containing an aluminum-only cathode. b) A representative aluminum-only cathode device fabricated from high M_n (Batch #H1) PBDTTPD with an initial performance of 6.9%. After 16 days of glovebox storage, the device performance is severely degraded.

We also fabricated devices using lithium fluoride as an interlayer between the active layer and the aluminum cathode. These unoptimized devices had lower initial PCEs (6.3%), and degraded in glovebox storage conditions (Fig. S8).

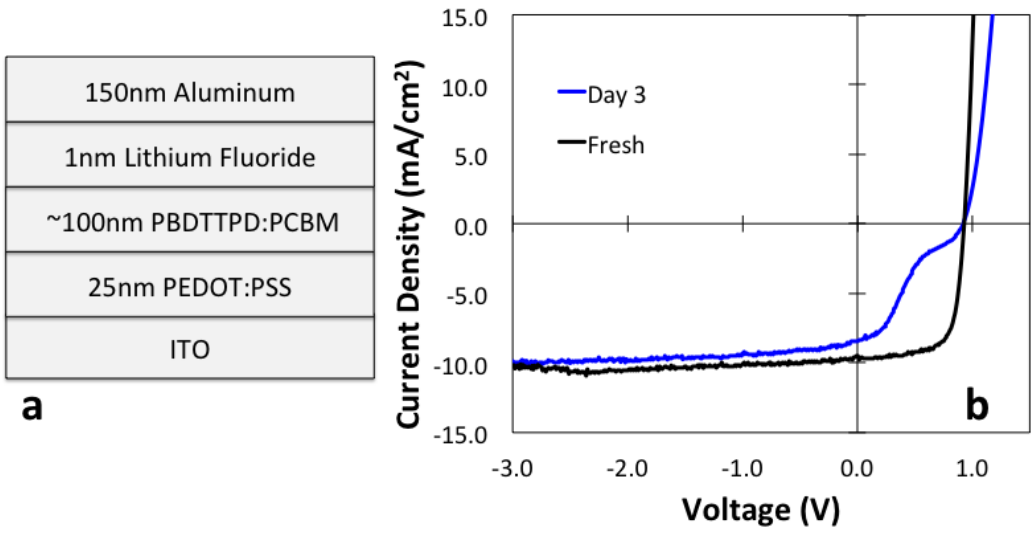

Figure S8: a) A schematic of a device containing a lithium fluoride interlayer and an aluminum cathode. b) J-V curves of a representative device fabricated from high M_n (Batch #H1) PBDTTPD using LiF/Al as the cathode. The initial PCE is 6.3%, and the device degrades substantially over three days of glovebox storage.

Finally, we tried using cesium carbonate as an interlayer between the active layer and the aluminum cathode. Unoptimized devices achieved initial PCEs of 5.4%, but again showed degradation in glovebox storage conditions (Fig. S9).

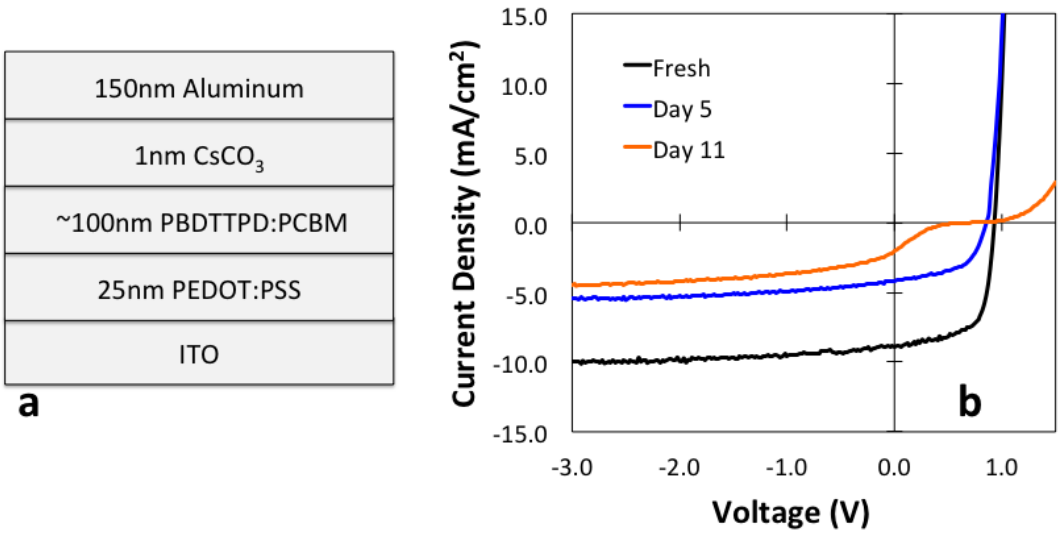

Figure S9: a) A schematic of a device containing a cesium carbonate interlayer and an aluminum cathode. b) J-V curves of a representative device fabricated from high M_n (Batch #H2) PBDTTPD showing an initial PCE approaching 5.4%. After several days of glovebox storage, the PCE degrades substantially.

Because removing or replacing calcium did not prevent degradation, we fabricated solar cells with a calcium/silver cathode. At 5.7%, the initial device PCEs were lower than with Ca/Al cathodes, and the devices suffered from a similar S-shape in reverse bias as the Ca/Al cathodes (Fig. S10).

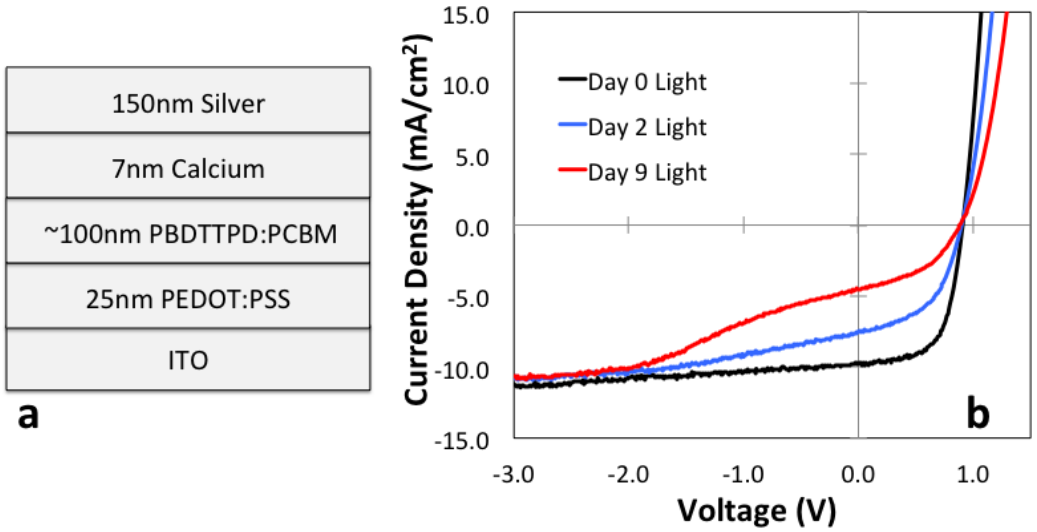

Figure S10: a) A schematic of a device containing a calcium hole blocking layer and a silver cathode. b) J-V curves of a representative device fabricated from high M_n (Batch #H2) PBDTTPD with a Ca/Ag cathode. The initial PCE approaches 5.8%, but the devices suffered from degradation in glovebox storage conditions. The S-shapes in reverse bias are very similar to the degradation symptoms observed in devices with Ca/Al cathodes.

Section 4: Processing Conditions

We also tried changing the device processing conditions (including annealing treatments) to prevent the S-shape degradation feature from appearing. We annealed films of high M_n PBDTTPD:$PC_{61}BM$ at 200°C for an hour before evaporating the calcium/aluminum cathodes. In addition to a reduction in initial PCE, we observed S-shape symptoms in annealed devices after they were aged for several days in the glovebox (Fig. S11).

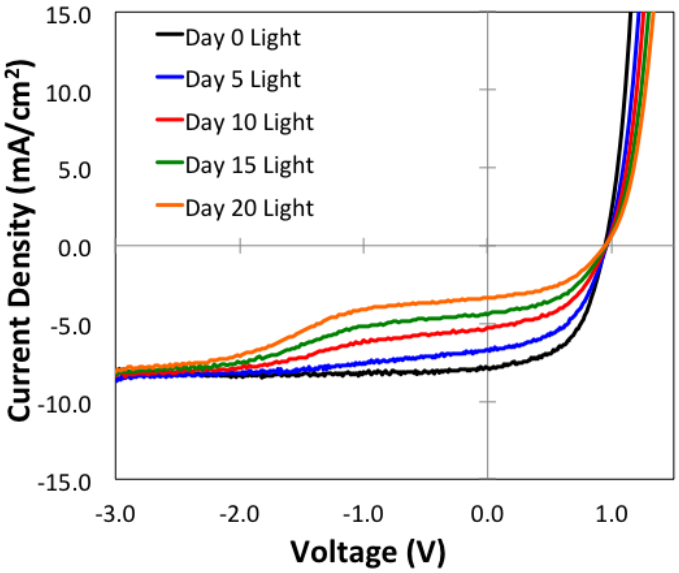

Figure S11: J-V curves of a representative high M_n (Batch #H2) PBDTTPD:$PC_{61}BM$ device that was annealed at 200° C for one hour before evaporation of a Ca/Al cathode. The initial PCE of annealed PBDTTPD:PCBM devices is substantially lower than non-annealed devices, and an S-shape grows with time in the reverse bias region.

In another experiment, we spun high M_n PBDTTPD:$PC_{61}BM$ onto an ITO/PEDOT:PSS anode and left the films in the glovebox at room temperature for 8 days before evaporating a calcium/aluminum cathode. Initial device performance was very similar to fully optimized, high M_n PBDTTPD:$PC_{61}BM$ solar cells, and approached 7.0%. These devices degraded on the same time scale as devices with immediately deposited cathodes (Fig. S12).

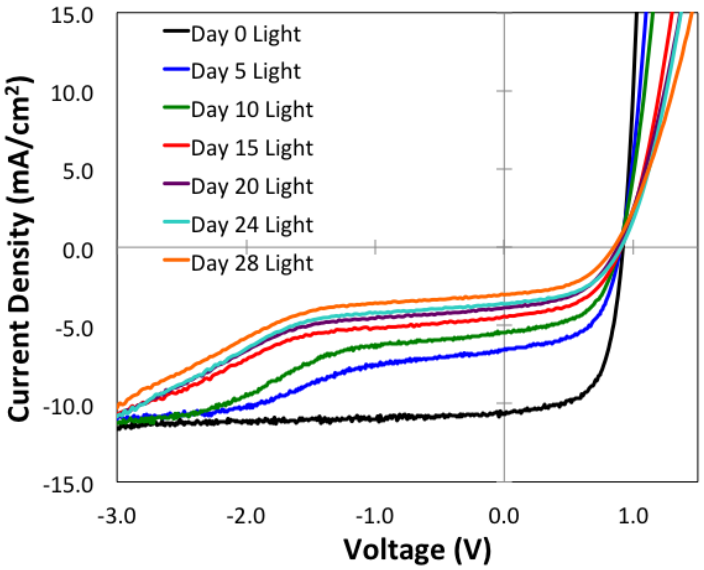

Figure S12: J-V curves of a representative high M_n (Batch #H3) PBDTTPD:$PC_{61}BM$ device that was left in the glovebox for 8 days before a Ca/Al cathode was evaporated. The initial efficiency is only slightly lower than fully optimized high M_n (Batch #H3) PBDTTPD:$PC_{61}BM$ solar cells. An S-shape in reverse bias appears after several days of glovebox storage and is seen to grow with time, on the same time scale as other Ca/Al devices.

Section 5: Estimating the Detection Limit of Organic Impurities Using Gas Chromatography-Mass Spectrometry

Low molecular weight organic impurities are not directly observed in the high M_n PBDTTPD samples by either size exclusion chromatography or gas chromatography-mass spectrometry (GC-MS) (Fig. S13). However, such impurities could exist within the sample, below equipment detection limits, and still cause widespread degradation (SI Sections 5 and 6). To determine if TPD was present in the high M_n PBDTTPD samples, the GC-MS detection limit for TPD was first determined.

A semi-concentrated sample of TPD in chloroform (100 μg/mL) was first investigated to determine the elution time of TPD. The GC spectrum shows that the retention time for TPD is about 14 minutes (Fig. S14a). Analysis of the spectrum presents a molecular ion of 422.9 M^+/z (mass to charge), which corresponds to the expected molecular ion for TPD (Fig. S14b).

To estimate the GC-MS detection limit of TPD, different concentrations of TPD were run through the equipment. The GC spectrum still showed a peak that corresponded to TPD (with a molecular ion of 422.9 M^+/z) when a concentration of 40 μg/mL was injected (Fig. S15). However, when the TPD concentration was reduced to 30 μg/mL, the GC spectrum did not show a peak at 14 minutes, nor a molecular ion of 422.9 M^+/z (Fig. S16). Thus, the GC-MS system has a detection limit of ~40 μg/mL TPD.

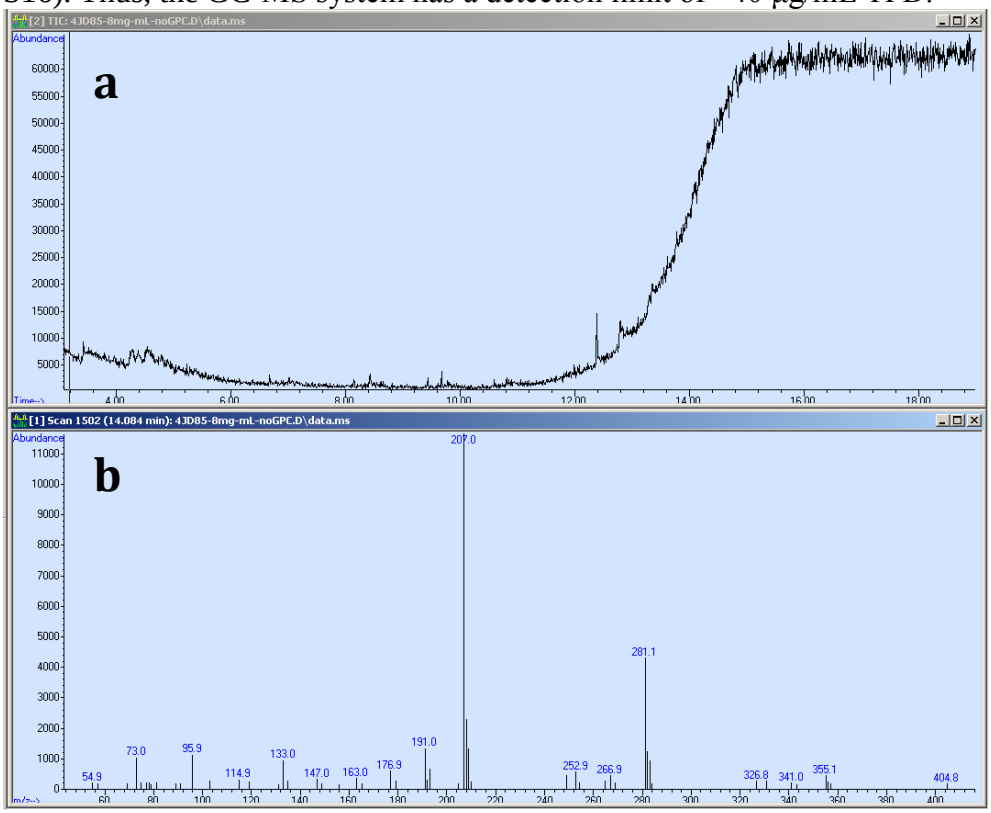

Figure S13: GC-MS spectra of 8 mg/mL high M_n PBDTTPD in chloroform. a) There is no peak at 14 minutes to indicate the presence of TPD. b) The molecular ion at 422.9 M/z, which corresponds to the molecular weight of TPD, is not present. No other peaks indicating large concentrations of any individual small molecule are clearly visible. However, such a molecule could exist at concentrations below the detection limit of the equipment.

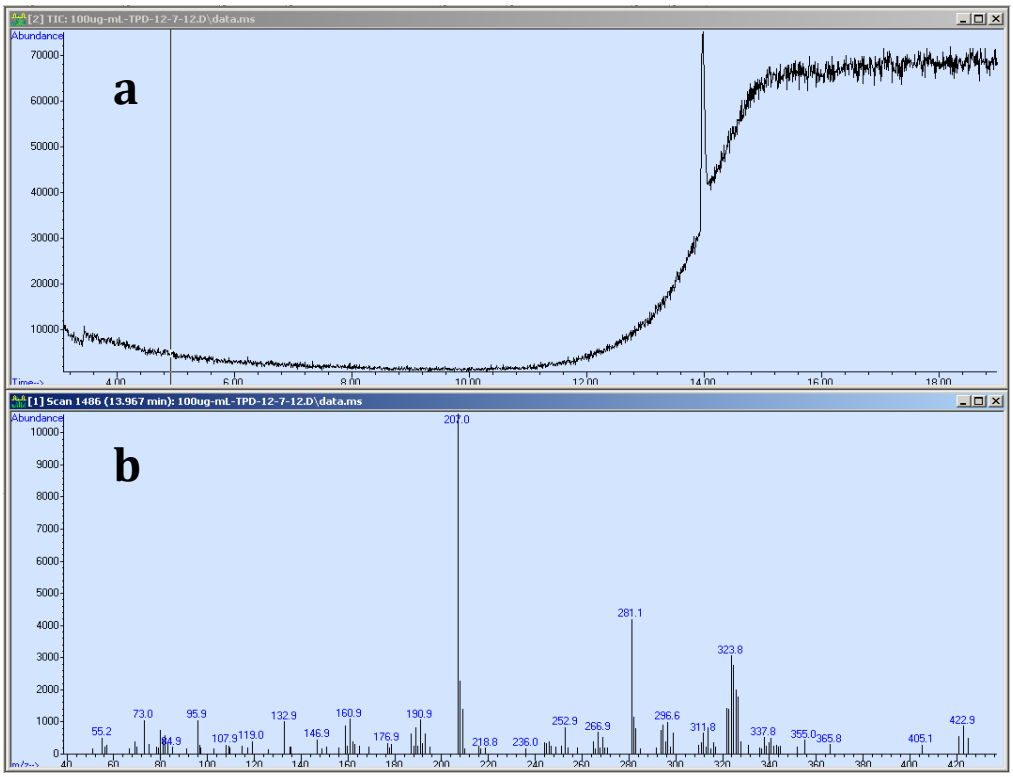

Figure S14: A semi-concentrated (100 µg/mL) solution of TPD in chloroform was run through the GC-MS to serve as a baseline for future experiments. a) A clear peak at 14 minutes establishes the elution time of TPD in chloroform. b) A molecular ion of 422.9 corresponds to the expected molecular weight of TPD.

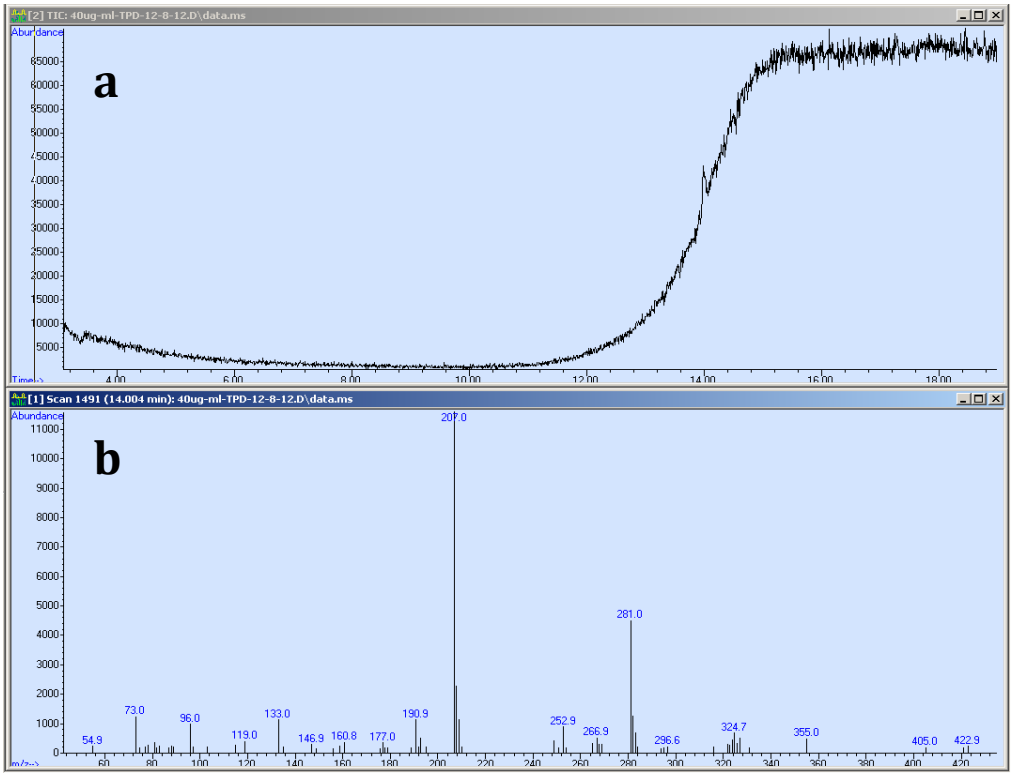

Figure S15: a) A TPD concentration of 40 µg/mL in chloroform still shows an elution peak at 14 minutes. b) A molecular ion of 422.9 M^+/z is also still visible.

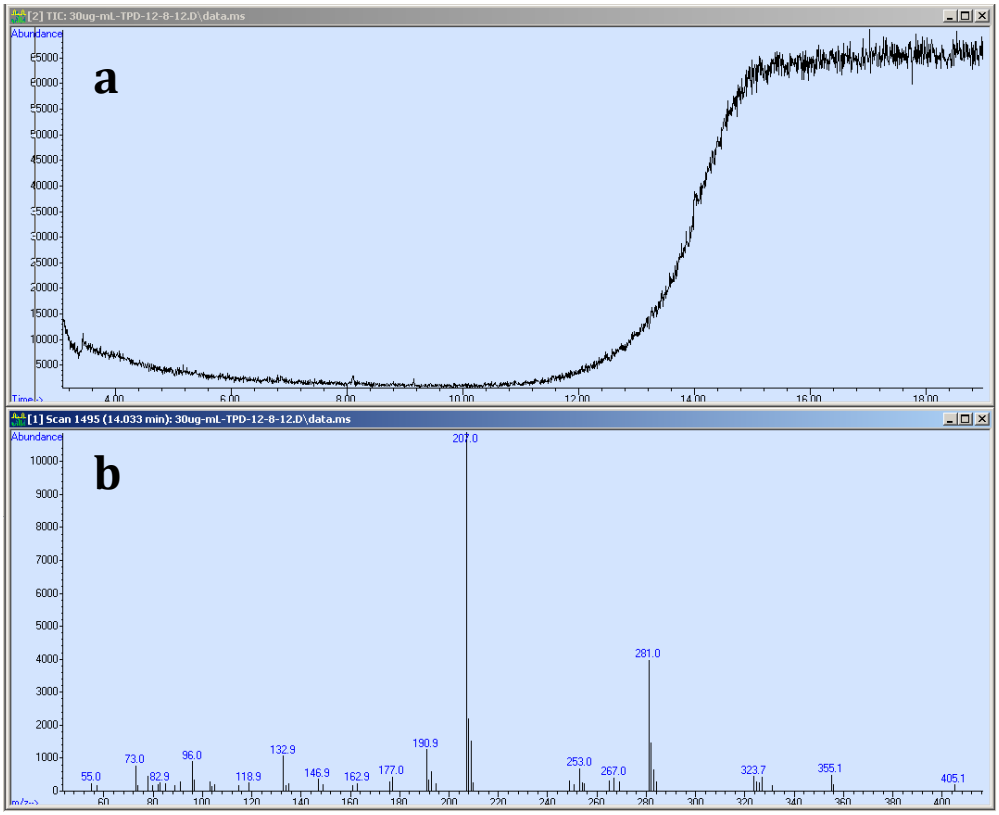

Figure 16: A TPD concentration of 30 µg/mL chloroform is below the equipment detection limits. a) No elution peak at 14 minutes, known to correspond to TPD, is detected. b) No molecular ion with M/z 422.9 is detectable.

Based on the results obtained from intentional contamination of low M_n PBDTTPD samples with TPD (in the manuscript), we estimate a total concentration of 12-120 µg/mL of low molecular weight impurities in high M_n PBDTTPD. Though the GC-MS detection limit of TPD is ~40 µg/mL, this is limit for *only* the potential TPD impurity. The total concentration of impurities in the high M_n PBDTTPD samples may exceed 40 µg/mL if there are multiple small molecule impurities.

GC-MS Instrumentation: GC-MS data was collected on an Agilent 7890A GC system fitted with an Agilent HP-5 chromatography column. Helium carrier gas at a flow rate of 2.2 mL/min was used as the mobile phase. The sample inlet was set at 250 °C and a pressure of 8.8 PSI was used to load the vaporized compounds onto the column at a split ratio of 50:1. The oven temperature was equilibrated at 50 °C for 30 seconds, and then a temperature program was run as follows: 50 °C for 1 minute, ramp to 310 °C at 20 °C/min, hold at 310 °C for 5 minutes. The total run time was 19 minutes. An auxiliary heater was kept at 150 °C between the GC column and the Agilent 5975C VL MSD system (electron impact (EI)), in order to keep the separated compounds from precipitating from the He carrier gas at the MSD system inlet. MS information was collected by the 5975C system and analysed with Agilent Chemstation software.

Section 6: Intentional Contamination with Organic Impurities

Table TS2: Average Initial Performance of Low M_n Devices with TPD contaminants

Added Monomer	PCE (%)	J_{SC} (mA/cm^2)	V_{OC} (V)	Fill Factor
0	4.83 (5.26)	-7.48 (-8.14)	0.97 (0.98)	0.66 (0.68)
0.1 mol.%	4.54 (5.12)	-7.09 (-7.92)	0.96 (0.98)	0.66 (0.68)
1.0 mol.%	4.14 (4.64)	-6.85 (-7.71)	0.95 (0.96)	0.63 (0.67)

( ) indicate maximum values

Section 7: TPD Monolayer Calculation

If an organic molecule (such as TPD) was to form a monolayer at the interface between the active layer and the cathode, it could pack in several different motifs. Most likely the molecules pack at an angle to each other to maximize interactions. However, there are two extreme cases – one in which the TPD molecules are completely upright and another in which the conjugated rings lie flat against the substrate surface (Fig. S17). In each case, we imagine that the carbon side chain would extend away from the surface. If the molecules pack in any of these configurations, the surface area per molecule would likely be something between 15-50 Å^2. We calculate the number of molecules needed to cover the substrate and the number of molecules in a dried film of PBDTTPD:$PC_{61}BM$:TPD (ES1, ES2).

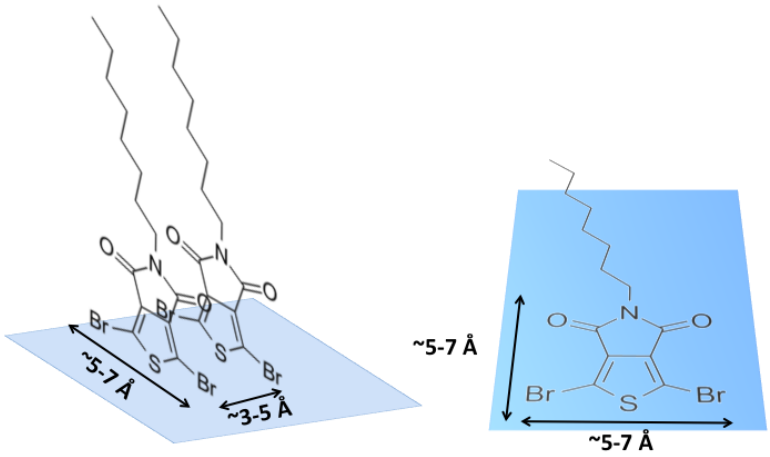

Figure S17: The extreme cases of packing orientations for a TPD monomer in a monolayer configuration, and the approximate dimensions of the molecular surface areas. These estimates do not imply knowledge of chemical interactions between the TPD monomer and the polymer or metal surfaces.

Equation ES1:

$$\frac{1\ molecule}{(0.15-0.50)\ \mathrm{nm}^2}\times\frac{(10^7\ nm)^2}{(1\ cm)^2}\times\frac{2.5\ cm^2}{substrate}\approx 5\times10^{14}-2\times10^{15}\left[\frac{molecules\ TPD}{substrate}\right]$$

Equation ES2:

$$1.0\%\ TPD\ \times\ (100\ nm\ \times\ 2.5\ cm^2)\times\frac{1\ TPD\ molecule}{(.150-.500)\ \mathrm{nm}^3}$$
$$\approx 5\times10^{14}-2\times10^{15}\ TPD\ molecules$$

Section 8: Size Exclusion Chromatography

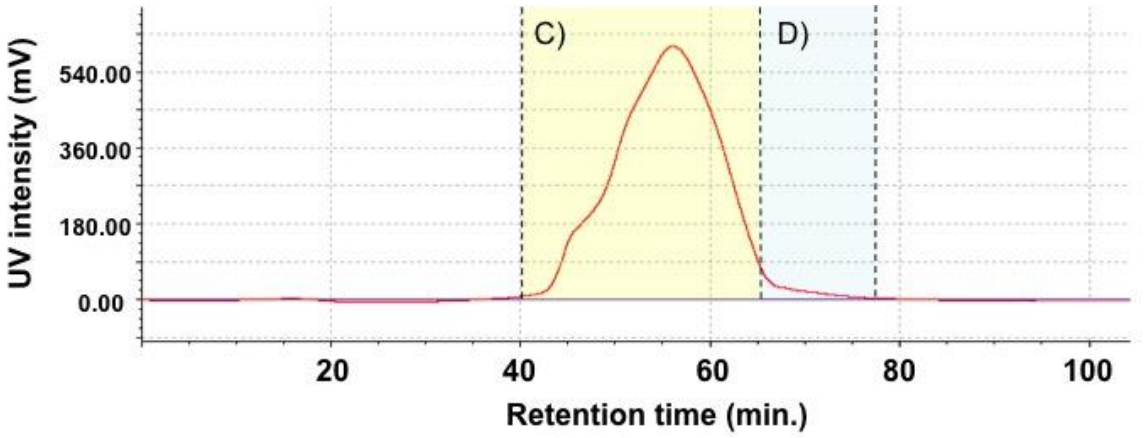

Figure S18: Elution pattern and fractionation of High *Mn* PBDTTPD (C=collected and D=excluded). Elution was carried out at room temperature with HPLC grade chloroform at a rate of 15 mL/min through a set of two JAIGEL-4H-40 columns mounted on a LC-9130NEXT (JAI) system; detection wavelength: 254 nm.

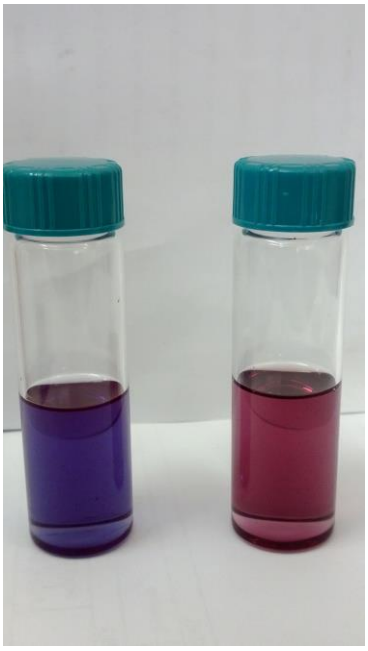

Figure S19: The solution absorption of the collected polymer fraction differs from that of the excluded fraction. A solution of collected polymer fraction, shown on the left, appears dark blue while a solution of excluded polymer, shown on the right, appears purple.